Advances in synchrotron radiation microtomography

José Baruchel, Jean-Yves Buffiere, Peter Cloetens, Marco Di Michiel, Emilie Ferrie, Wolfgang Ludwig, Eric Maire, Luc Salvo

Advances in synchrotron radiation microtomography

José Baruchel,[a,*] Jean-Yves Buffiere,[b] Peter Cloetens,[a] Marco Di Michiel,[a] Emilie Ferrie,[b] Wolfgang Ludwig,[a,b] Eric Maire[b] and Luc Salvo[c]

[a]*ESRF, Experimental Division, BP 220, 6 Rue Jules Horowitz, 38043 Grenoble Cédex, France*
[b]*GEMPPM, INSA Lyon, 69621 Villeurbanne Cédex, France*
[c]*GPM2, INPG, BP 46, 38402 Saint Martin d'Hères, France*

Abstract—The use of synchrotron radiation X-ray microtomography rests on the exploitation of the beam coherence, the high spatial (submicron) or temporal resolution (s), in situ and real time experiments and quantitative measurements. Selected original applications showing these capabilities are presented. They include the phase contrast imaging of Si particles in Al alloys, the nucleation of fatigue cracks in structural materials, the visualization of hollow silica spheres within polymer foams, and the real time observation of the semi-solid state in Al–Cu alloys.

Keywords: Synchrotron radiation; Image analysis; Fracture; Microstructure; Solidification

1. Introduction

There are many variants of synchrotron radiation (SR) based X-ray imaging, including micro-spectroscopy [1], and three-dimensional (3D) imaging based on absorption, scattering [2] or phase, using, in this last case, the coherence of the SR beams. X-ray imaging techniques are non-destructive and can be selective for a wide range of properties (density, chemical element, chemical bond, strain, surface versus bulk, order versus disorder), with extremely high sensitivity. These techniques are revolutionising the perceptions in the scientific community of the possibilities offered by SR.

The present paper is devoted to the evolution of synchrotron radiation X-ray microtomography, characterized by an increased use of (i) phase contrast imaging, (ii) high spatial or temporal resolution, (iii) in situ experiments using adapted sample environment, and (iv) precise quantitative measurements.

Synchrotron radiation microtomography basically consists of recording a series of radiographs (typically of the order of 1000) for different angular positions of the sample, which rotates around an axis perpendicular to the beam. Several successful laboratory microtomographs have been commercially produced over the last years [3,4] but the best images, in terms of spatial resolution, signal-to-noise ratio and quantitative exploitation, are obtained using SR. This results from the high intensity (multiplied by 10^6 with respect to usual X-ray generators), practically parallel and monochromatic incoming beam, the availability of photons spanning the whole range from the infrared to hard X-rays (up to 300–400 keV) and the high degree of coherence of the beam.

In the usual SR microtomographic approach there is no image magnification, and the spatial resolution mainly results from the effective pixel size of the detector, now in the μm range. The total acquisition time is in the 10^{-3} (''fast tomography'') to 1 h range, and the recorded data often amounts to several gigabytes.

2. Advances in phase contrast microtomography: the example of Al–Si

The X-ray beams produced at modern synchrotron radiation facilities exhibit a high degree of coherence. This results from the small angular source size α seen from one point of the sample ($\alpha < \mu$rad). It leads to a transverse coherence length $d_c = \lambda/2\alpha$ in the 10^{-4} m range, and to ''phase images'', the contrast arising from phase variations across the beam transmitted through

* Corresponding author. Tel.: +33 4 76 88 21 01; fax: +33 4 76 88 25 42; e-mail: baruchel@esrf.fr

the sample. Phase images are recorded by just varying the sample-to-detector distance: this is the "propagation technique", reviewed for instance in Ref. [5]. The great advantage of phase contrast imaging is the increased sensitivity it provides, either for light materials or for composites made up of materials with similar densities (for example Al and Si alloys).

A first, qualitative, use of the phase images relies on the visualization of the phase jumps that occur at the edges of a particle or porosity imbedded in a matrix having a different index of refraction. This edge-detection regime occurs for a sample-to-detector distance smaller than $d^2/2\lambda$, where d is the typical size of the features we wish to observe, and λ is the wavelength of the incoming monochromatic X-ray beam. This edge-detection approach is illustrated in Figure 1a which shows the images of small (1–5 μm) Si inclusions within a virtual slice, extracted from the 3D image, of a 0.3 mm diameter cylindrical sample of a cast Al alloy AS03G7. The image contrast is governed by the 'edge-enhancement' as indicated by the plot (Fig. 1c, corresponding to the region indicated by a white rectangle in Fig. 1b) that clearly shows the particle edges being underlined by a black-white fringe pattern. These particles, with sizes close to the resolution limit of our setup (detector pixel size 0.4 μm) are practically not observable when only using absorption contrast because, at the chosen X-ray energy of 10.7 keV (corresponding to a 15% standard transmission in X-ray tomography), the contrast of the images of the largest particles only amounts 3%.

Phase imaging based on the detection of the edges does not allow the quantitative extraction of the local phase, and its spatial resolution is limited by the occurrence of the fringes used to visualize the borders. Cloetens and co-workers developed a quantitative approach, called holotomography, allowing phase retrieval through the combination of several images recorded at different distances [6]. The highest accessible spatial frequency is not limited by the technique, and is only determined by the resolution of the detector. Figure 2 shows the result of applying the "holotomographic" procedure to the same Al alloy: the two phases are clearly observable through their grey level. The refractive index decrement measured in Figure 2b and c is, to a very good approximation, proportional to the density difference and can provide a map of the mass density in the sample.

Figure 3 shows two volume renderings of the microstructure of the investigated material. The contrast in the holotomographic reconstruction allows the use of a simple threshold algorithm to visualize only the Si

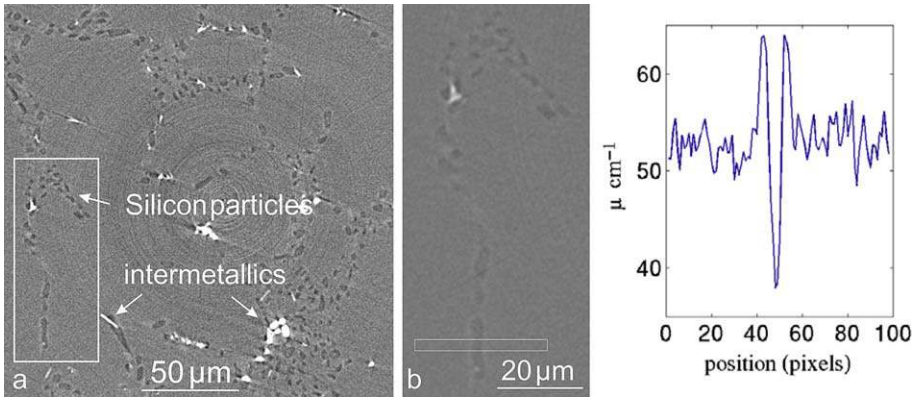

Figure 1. (a) Phase sensitive tomograph showing the microstructure of as cast Al alloy; (b) detail showing individual Si particles; (c) plot of the image intensity in the rectangular box across the elongated Si particle at the bottom of (b), illustrating the edge-enhancement effect.

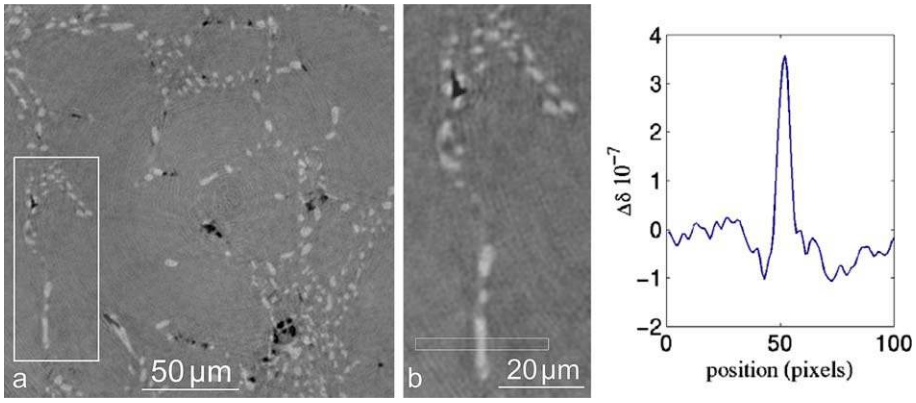

Figure 2. Quantitative reconstruction of the refractive index distribution using the holotomographic approach (same region as Fig. 1). Improved image contrast and resolution allow for detection of small Si particles down to 1–2 μm size. The strong difference in the refractive index decrement (see plot) allows for straightforward image segmentation and analysis.

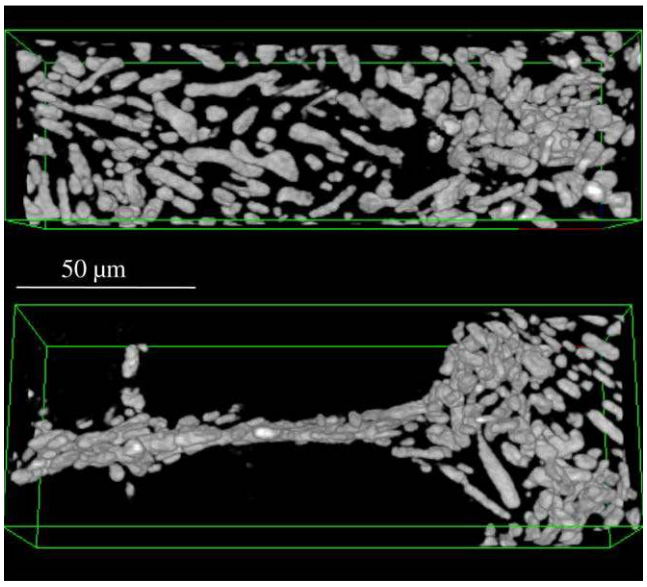

Figure 3. Two 3D renditions showing the arrangement of the Si particles in the grain boundaries of the as cast solidification microstructure.

particles. This reveals the preferential location of these particles, formed during the solidification of the eutectic phase between the dendrites of the primary Al, on the grain boundaries.

3. Improved spatial resolution: imaging thin features

Phase microtomography is well adapted to provide 3D information on features like cracks, porosities or inclusions. Nucleation of cracks requires the microstructure to be observed at the highest possible spatial resolution. As the SR X-ray beam is nearly parallel, the resolution is directly linked to the detector pixel size. When using a scintillator and a visible light charge-coupled device (CCD) camera, the pixel size is limited by the diffraction to about $\lambda/2$ for the visible photons, i.e. presently 0.28 μm on the ID19 beamline of the ESRF. This is enough to approach phenomena like the nucleation of thin fatigue cracks in structural materials.

Characterizing the growth of small fatigue cracks is an important scientific issue because in some cases (low stress levels, high cycle fatigue) it corresponds to a substantial part of the fatigue life of a component (examples can be found in most of the components subjected to a fatigue loading like wings or skins in aircrafts, rails, car wheels, bearings). However, experimental data in this field is scarce and model predictions are therefore difficult to validate.

High resolution X-ray tomography has been used to obtain in situ successive images of growing fatigue cracks in metals, using a voxel size of 0.7 μm. With this voxel size, it should, in principle, not be possible to image crack tip opening displacement, in the 10^{-1} μm range, even for a sample under load. But the use of phase contrast helps to improve damage detection down to about 0.1 μm. It is therefore possible to obtain a good description of the crack shape, comparable to that obtained by optical microscopy. As a matter of fact, a voxel size of 0.7 μm is a compromise between the need for a high resolution, the minimum size of a fatigue sample (cross section 1×1 mm^2), and the requirement that the projections should fit on a 2048×2048 CCD detector. Figure 4 shows reconstructed images of a small crack growing inside a cast Al alloy. The sample is cycled in situ and successive scans are recorded after applying several thousands of fatigue cycles.

The analysis of several similar 3D images has shown that the growth of small fatigue cracks is influenced by the presence of grains, which induce an irregular crack front. In Al alloys the grain boundaries can be visualized in 3D by tomography with a Ga infiltration technique [7,8]. This irregular shape is a key factor to be taken into account for modeling as it implies that the stress intensity factor K varies along the crack front. However, the growth in the different grains is not completely independent and the crack front remains coherent. This is the result of a balance between an increase of the local stress intensity factor value on the parts of the crack front that are retarded, and a decrease on the ones that are protruding. When the crack size increases, the crack front shape tends to be more regular but the transition towards a uniform K-related shape and a "long crack" growth has not been observed so far because of the limited number of grains present in the small cross

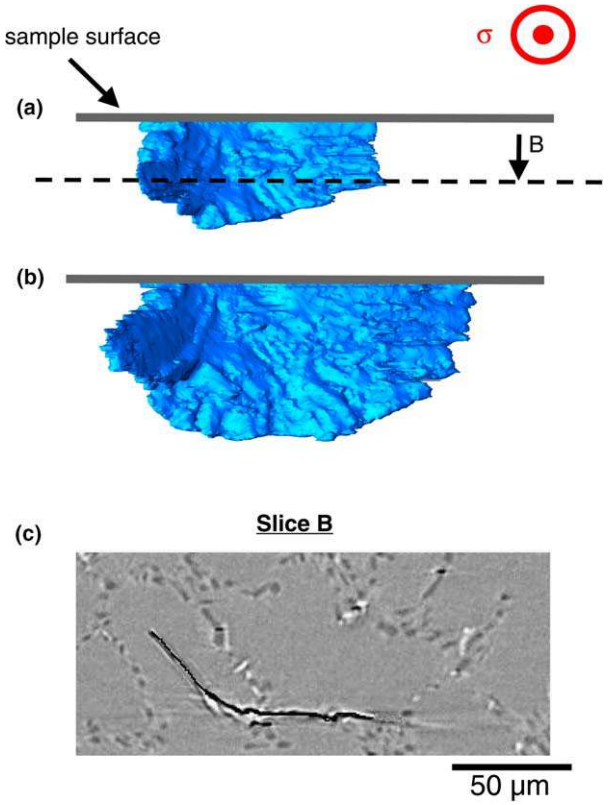

Figure 4. Images of a fatigue crack growing from the surface inside a cast Al alloy: (a) 3D rendering of the crack surface as seen along the stress direction after 270,000 fatigue cycles; (b) after 285,000 fatigue cycles; (c) reconstructed 2D slice (along B, as indicated in (a)) showing a strong deviation of the crack front (underlined in black for clarity) induced by a grain boundary (not directly visible on the *image*).

section of the specimens studied. Complementary experiments with an ultrafine grained Al Li alloy have been carried out recently [9]; they bring new quantitative data on the crack growth of long fatigue cracks in relation to 3D fatigue crack closure.

High resolution is also required when the features of the microstructure to be analyzed have a very small size. An illustration of such a situation is the case of the syntactic foams used in the oil industry to thermally insulate the pipes transporting hot oil from the extraction fields situated at a high depth in the cold sea water. While they need to prevent the oil cooling down, these materials also have to resist a 30 MPa hydrostatic pressure. They are composed of a polymer matrix surrounding hollow silica spheres reinforcing the porous structure and preventing it collapsing under the applied pressure. Due to their heterogeneous nature, these materials (composed of air, silica and polymer) are extremely difficult to observe using standard microscopy techniques and X-ray tomography has been successfully used recently for this purpose [10]. The determination of the thickness of the hollow spheres is very important for the understanding of the physical properties of this material. But this thickness typically lies in the range 1–3 μm. Thus the most appropriate way to determine it has been to use the 0.28 μm resolution available at the ESRF. An illustration of the type of microstructure obtained for these materials, using this setup, with two different voxel sizes, is shown in Figure 5. This figure is composed of two reconstructed slices of the same sample at the same location but with the 0.7 μm (left image) and the 0.28 μm (right image) resolution setups. One can clearly notice that the thickness of the silica hollow spheres is very small and requires the best available spatial resolution.

Great efforts are currently being put into enhancing the spatial resolution below the 100 nm range, but this implies producing an X-ray spot size of a few tens of nm. This technique was recently applied to understanding the propagation of liquid Ga in an Al alloy [11].

4. Enhanced temporal resolution: the example of semi-solid Al–Cu alloys

Semi-solids alloys are important materials for applications. The understanding of their mechanical properties involves knowing the 3D arrangement of both the solid and liquid phases. This was performed on Al–Si and Al–Cu alloys by SR microtomography at room temperature on rapidly quenched samples [12–14]. A strong assumption made in conducting such experiments is that quenching is fast enough to retain the semi-solid arrangement present at high temperature. This assumption was shown to be incorrect through recent ultrafast microtomographic experiments that allow the 3D microstructure to be obtained without the need for quenching as shown in Figures 6 and 7. One can see that after quenching, more solid (in dark grey) is present and thus every structural parameter that can be measured for the quenched sample (solid fraction, interface area between solid and liquid, solid morphology, etc.) will be different from what it really is in the semi-solid state. In situ, fast tomography experiments are thus mandatory to characterize the microstructure in the semi-solid state.

These in situ experiments in the semi-solid state (during isothermal holding or even solidification path) are now possible with a 2.8 μm pixel size thanks to a specific ultrafast device. A complete scan with a specimen of 1.5 mm diameter and 1.5 mm height, performed using a 512×512 pixels CCD camera and recording 500 radiographs (with 20 m s exposure time/radiograph) requires only 10 s. This technique has been used for the study of isothermal holding in the semi-solid state of Al–Cu alloys [15] and also the study of in situ equiaxed solidification of Al–Cu alloy [16].

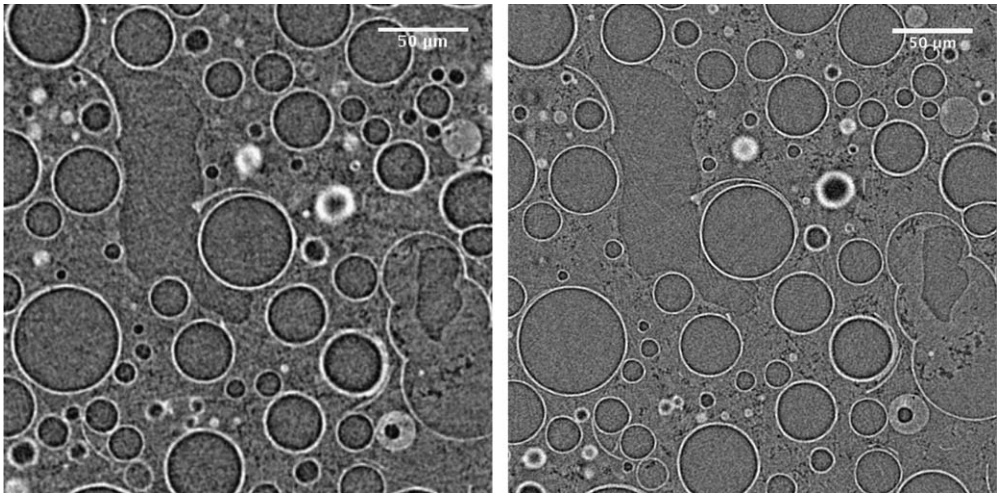

Figure 5. Comparison of the same reconstructed tomographic slice ($E = 20.5$ keV, sample-to-detector distance 15 mm) of a polymer foam containing hollow silica spheres used in the oil industry as thermal insulation in deep-sea water. The left one was recorded using a 0.7 μm voxel size, whereas a 0.28 μm voxel size was used for the right one: this shows that the highest spatial resolution is required to image the very thin silica thickness of the reinforcement.

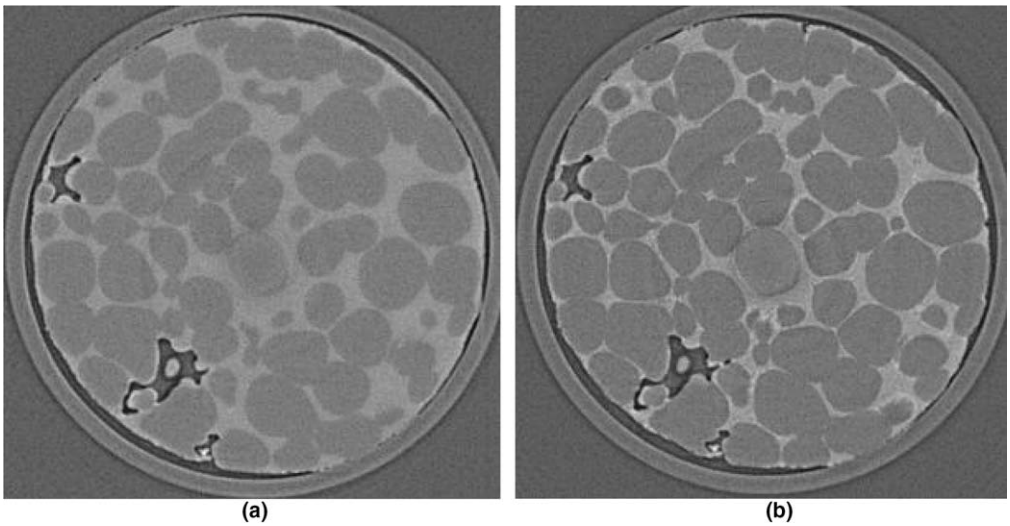

Figure 6. (a) 2D section extracted from 3D data obtained during in situ isothermal experiments of an Al–15.8 wt.%Cu alloy in the semi-solid state. The specimen diameter is 1.5 mm. (b) As per (a) but after rapid quenching. The comparison of (a) and (b) shows that quenching from the solid state to room temperature leads to an increase in the fraction of solid particles.

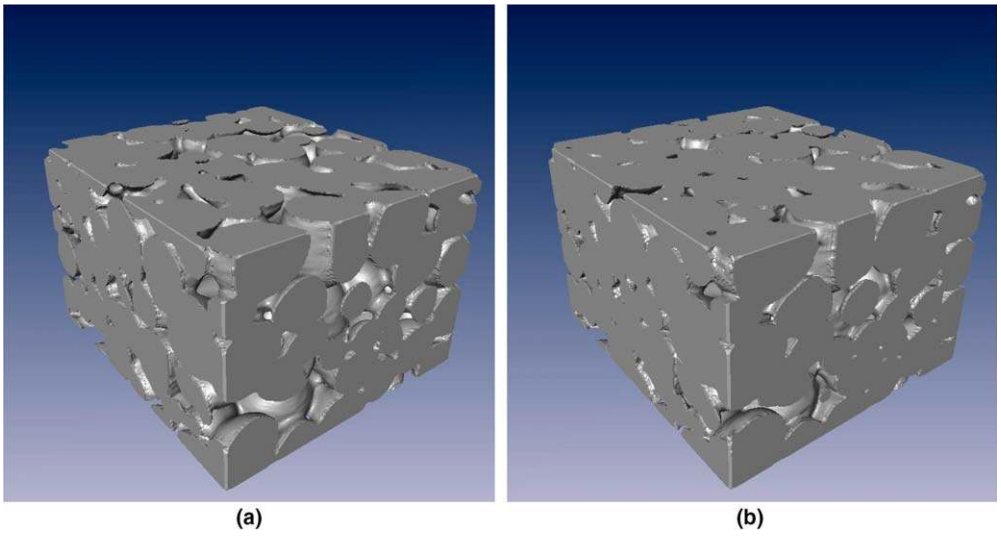

Figure 7. (a) 3D rendering of an Al–Cu alloy in the semi-solid state (see Fig. 6a) (imaged height ~0.6 mm). (b) 3D rendering of sample shown in (a) quenched from the semi-solid state (see Fig. 6b) (imaged height ~0.6 mm).

5. Present state and future developments

The above examples show the potential of SR X-ray microtomography in experiments using the beam coherence, for "fast tomography" to investigate the evolution of a system when varying an external parameter (time, temperature, stress, etc.) and/or for improved spatial resolution, which is currently reducing towards the 100 nm range.

Most of the previously described microtomographic experiments imply specially designed sample environment cells: furnace, traction machine. Effort is being pursued in this direction, specific attention being paid to the measurement of the temperature of the specimen during the experiment and to the control of the thermal gradient. A high temperature tensile device is being designed.

Another important feature is the quantitative extraction of data from the images. This quantification can be performed through the inclusion of markers in the sample, and the study of the evolution of these markers location during the deformation. This provides a very good image of the strain field within the sample, as shown by Nielsen and co-workers [17].

The use of monochromatic beams allows a quantitative extraction of the local density within the 3D sample to be performed. Peyrin and co-workers carried out this demanding quantitative work to detail the mineralization of bones and its evolution under the action of drugs delivered to reduce osteoporosis [18–20]. This type of experiment will surely extend to materials science, for instance to distinguish between phases in a complex alloy.

It is clear that these SR-based 3D X-ray imaging methods will increasingly develop over the next years,

both from the point of view of the improvement of the technique and in terms of the domains of application. The spatial resolution, presently in the 100 nm to 1 μm range, is being pushed to gain one order of magnitude. Temporal resolution is being improved to the few seconds range for a complete 3D scan, to investigate evolving processes like fracture propagation or phase transformations. Examples of new research subjects include of course materials science, where the entire range of length scales (~50 nm to 50 mm) can be covered, nano-technology where the important scale is 50 nm and below, as well as new areas of interest like medicine, environmental sciences, archaeology, palaeontology, and human heritage sciences.

Acknowledgements

The authors wish to thank Elodie Boller (ESRF) for assistance during the experiments and Françoise Peyrin (CREATIS-INSA) for discussions on the quantitative extraction of the local density from the 3D images. The images of syntactic foams were obtained with the help of Valérie Sauvant Moynot (IFP), Henry Sautereau and Nelly Gimenez (LMM) and Jerome Adrien (GEMPPM).

References

[1] F. Adams, K. Janssens, A. Snigirev, J. Anal. At. Spectrom. 13 (1998) 319.
[2] B. Golosio, A. Simionovici, A. Somogyi, M. Lemelle, M. Chukalina, A. Brunetti, J. Appl. Phys. 94 (2003) 145.
[3] P. Rüegsegger, B. Koller, R. Müller, Calcified Tissue Int. 58 (1996) 24.
[4] A. Sasov, D. Van Dyck, J. Microsc. 191 (1998) 151.
[5] P. Cloetens, W. Ludwig, J. Baruchel, J.P. Guigay, P. Rejmankova-Pernot, M. Salomé-Pateyron, et al., J. Phys. D: Appl. Phys. 32 (1999) A145.
[6] P. Cloetens, W. Ludwig, J. Baruchel, D. Van Dyck, J. Van Landuyt, J.P. Guigay, et al., Appl. Phys. Lett. 75 (1999) 2912.
[7] W. Ludwig, J.Y. Buffière, S. Savelli, P. Cloetens, Acta Mater. 51 (2003) 585.
[8] K.H. Khor, J.Y. Buffière, W. Ludwig, H. Toda, H.S. Ubhi, P.J. Gregson, et al., J. Phys.: Condens. Matter 16 (2004) S3511.
[9] E. Ferrié, J.Y. Buffière, W. Ludwig, A. Gravouil, L. Edwards, Acta Mater., in press.
[10] E. Maire, N. Gimenez, V. Sauvant-Moynot, H. Sautereau, Philos. Trans., in press.
[11] E. Pereiro Lopez, W. Ludwig, D. Bellet, P. Cloetens, C. Lemaignan, Phys. Rev. Lett. 95 (2005) 215501.
[12] S. Verrier, M. Braccini, C. Josserond, L. Salvo, M. Suéry, P. Cloetens, J. Baruchel, in: Baruchel, Buffière, Maire, Merle, Peix (Eds.), X-ray Tomography in Material Science, HERMES Science Publications, Paris, 200, 2000, p. 77.
[13] S. Verrier, M. Braccini, C. Josserond, L. Salvo, M. Suéry, P. Cloetens, W. Ludwig, in: Chiarmetta, Rosso, Edimet, Brescia (Eds.), Proceedings of the Sixth International Conference on Semi-solid Processing of Alloys and Composites, Turin, Italy, 2000, p. 771.
[14] L. Salvo, P. Cloetens, E. Maire, S. Zabler, J.J. Blandin, J.Y. Buffière, et al., Nucl. Instrum. Methods Phys. Res., B 200 (2002) 273.
[15] L. Salvo, M. Pana, M. Suéry, M. DiMichiel, Ø. Nielsen, D. Bernard, in: L.K.R. Helmut Kaufmann (Ed.), Proceedings of the Second International Light Metals Technology Conference 2005, 2005, p. 209.
[16] O. Ludwig, M. Di Michiel, L. Salvo, M. Suéry, F. Falus, Metall. Mater. Trans. 36A (2005) 1515.
[17] S.F. Nielsen, H.F. Poulsen, F. Beckmann, C. Thorning, J.A. Wert, Acta Mater. 51 (2003) 2407.
[18] S. Nuzzo, F. Peyrin, P. Cloetens, J. Baruchel, G. Boivin, Med. Phys. 19 (2002) 2672.
[19] S. Nuzzo, M.H. Lafage-Proust, E. Martin-Badosa, G. Boivin, T. Thomas, C. Alexandre, et al., J. Bone Miner. Res. 17 (2002) 1372.
[20] E. Martín-Badosa, D. Amblard, S. Nuzzo, A. Elmoutaouakkil, L. Vico, F. Peyrin, Radiology 229 (2003) 921.